COMMUNICATION

Development of a Microfluidic Device to Investigate Cancer Metastasis

Megan M. Parsons,[a] Jack Zhou,[b] Jaden Tayag,[a] and Raunaq Zamal[a]

Received 28th April 2020,
Accepted 00th January 20xx

DOI: 10.1039/x0xx00000x

Metastasis is a major predictor of morbidity and mortality in cancer patients, but the details of this process are poorly understood. Here we report the design and characterization of a microfluidic assay developed to quantify the proliferative index of metastatic breast cancer cells and elucidate their molecular and genetic features. These data can be used to develop novel therapeutics to target and inhibit specific stages of metastatic progression.

Cancer metastasis is responsible for marked decreases in patient survival.[1] Metastasis is the process through which cells from a primary tumor enter the bloodstream or lymphatic system and form secondary tumors at distant sites. Despite recent advancements in cancer diagnostics and therapeutics, many patients experience metastatic events prior to an initial cancer diagnosis, and most cancer deaths are attributed to the growth and proliferation of treatment-resistant metastases.[2] Furthermore, it is unlikely that the efficacy of a single drug will be sufficient to prevent metastatic spread of cancer, and scientists would benefit from high-throughput drug screening methods to pursue these combinatorial studies.[1]

The pathogenesis of metastasis is a highly complex process that consists of 11 necessary, sequential steps[2]:

1. Carcinogenesis is initiated via an oncogenic transformation event. This event elicits genetic and phenotypic changes in cells at the primary tumor site.

2. Angiogenesis allows for the formation of new blood vessels to supply the tumor with oxygen and nutrients needed to grow and proliferate.

3. Tumor invasion of the stroma causing evolution of the extracellular matrix and adaptation of the tumor microenvironment.[3]

4. Tumor cells undergo intravasation into the bloodstream to become circulating tumor cells (CTCs).

5. The majority of tumor cells in the bloodstream are rapidly destroyed, but a few successfully evade the immune system and survive.

6. The surviving, circulating tumor cells then arrest in the capillary beds of organs.

7. Tumor cells proliferate within the capillary vessels.

8. Tumor cells undergo extravasation into the organ tissue.

9. A metastatic site is established as tumor cells grow and proliferate within the organ parenchyma.

10. Angiogenesis provides a blood vessel network to the growing tumor to supply oxygen and nutrients supporting proliferation.

11. The newly formed tumor must continue to evade the host's immune system to continue to grow and thrive.

Better understanding this process is a primary goal of cancer research. To this end, we have designed a microfluidic assay to probe these details in the formation of secondary tumors in the brain tissue of breast cancer patients.

For our microfluidic design, we chose to focus on recapitulating three key elements involved in metastatic cancer spread: (1) the biochemistry and biophysics of the tumor microenvironment (TME); (2) unidirectional, pulsatile fluid flow simulating human

[a] *Department of Electrical & Computer Engineering, Boston University, Boston, MA, USA.*
[b] *Department of Biomedical Engineering, Boston University, Boston, MA, USA.*

systemic circulation; and (3) an approximated blood-brain barrier separating healthy brain tissue from the blood circulation.

The microfluidic device design consists of a circular vascular structure containing an inlet, outlet, tissue-vascular interfaces, and valve-less pump. The inlet allows for continuous infusion of oxygen and nutrients, while the outlet allows for by-product waste removal. Adjacent to the primary circulation is a switch-activated dielectrophoresis (DEP) sorter, which allows for the separation and downstream analysis of circulating tumor cells (CTCs). Table 1 summarizes the device dimensions. A device overview can be found in Figure 1.

The valve-less pump in our device allows for unidirectional, pulsatile, multi-phase fluid flow.[4] This simulates the natural blood pumping mechanism of the human heart. Furthermore, this pump is able to be modulated to represent a range of cardiovascular states, like hypertension or states of modulated fluid flow (~1-500 nL/s).[4] This enables flexibility in the research parameters for any given assay.

The tissue-vascular interfaces consist of a primary tumor site and a potential metastatic site. Both sites interface with channels representing thin-walled venules. The primary tumor site in our microfluidic model consists of a well containing MDA-MB-231 breast cancer cells. MBA-MB-231 cells are a commonly used, aggressive, invasive, triple-negative human breast cancer subtype with limited treatment options and a propensity to metastasize to the brain.[5] This well should be seeded at 1 * 10^4 cells/cm^2, held at 37˚C in Leibovitz's L-15 medium + 2 mM glutamine and 15% fetal bovine serum (FBS), and split (subcultured) when 80% confluent.[5] The other well contains a sophisticated blood-brain barrier (BBB) multicellular environment consisting of human iPS-BMVECs, human pericytes, and human astrocytes prepared using developmentally-inspired, state-of-the-art protocols (with potential experimental optimizations to account for differences in microfluidic design).[6] The overall design of this segment of the chip is based on a simpler, predicate model.[7] In the predicate model, there is a layer of glass, covered by PDMS containing the organ chambers, which is covered by a porous membrane, and finally topped with a PDMS layer containing microchannels.[7] We are proposing a modified model in which the porous membrane is adjusted, as the primary interface between the chambers and fluid flow is now biological. The

Component	Length	Width	Height	Spacing
Channels/ Connections		400um	60/120/240um	
Chambers	2000um	5000um	250um	
Valves	2000um	1000um	250um	
Pump	300um	100um	250um	1000um

Table 1. Microfluidic device dimensions. N.B.: Channel height specifies bio-mimicking capillary (60 µm), vein (120 µ), and artery (240 µm) dimensions.

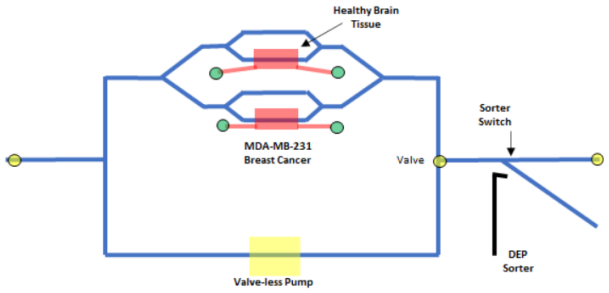

Figure 1. Overview of microfluidic device, including valve-less pump, tissue wells and fluid interfaces, and DEP sorter.

microchannels can be used in the delivery of biochemicals, like chemokines, that are customarily used in these experiments. The primary channels are therefore used as a circulatory system proxy, and as such, both the microchannels and primary channels will be lined with human umbilical vein endothelial cells (HUVEC) and coated with Basement Membrane Extracts (BME), as described in Kong, et. al.[7]

Although the lymphatic system may provide an alternative point of entry for cancer cells into the circulation, the extensive network of vasolymphatic cross-connections renders this distinction invalid; therefore, we chose to focus on microfluidic channels representing vasculature exclusively.[2]

The inclusion of the DEP sorter was intended to enhance research on the effects of CTCs in non-metastatic breast cancer. Research has shown that the presence of CTCs in non-metastatic breast cancer patients indicated a poorer prognosis and a lower likelihood of overall survival.[8] Studying the genetic and phenotypic characteristics of CTCs can further our understanding of prognostic indicators, cancer biomarkers, and potential drug targets.

There are many benefits to this microfluidic research platform. Traditional *in vivo* studies of metastatic cancer will use model systems, like zebrafish, and transplant human tumor cells to investigate cellular migration.[9] However, vital human-specific tumor microenvironment parameters are absent from these studies, so nuanced biochemical and biophysical analysis isn't possible in these systems. Alternatively, conventional *in vitro* models are able to mimic human tissue environments more closely and provide stricter control over experimental parameters. However, traditional assays like the Boyden chamber lack control over experimental parameters and pose challenges in imaging and quantification of cells.[10,11] Our proposed microfluidic research platform boasts two separate, controllable biological microenvironments, a biologically-inspired tissue-vascular interface, and a bio-mimicking circulation.

3DuF is an open-source, interactive design tool for specifying microfluidic designs.[12] A 3DuF rendering of our microfluidic device is shown in Figure 2.

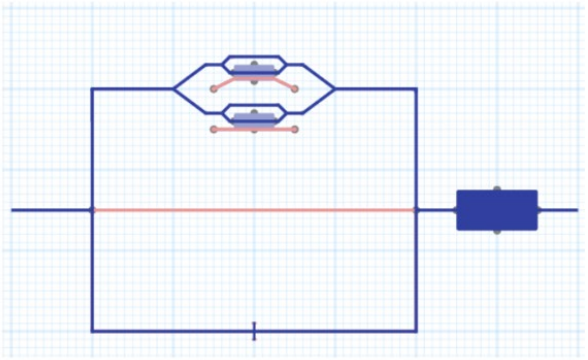

Figure 2. A 3DμF rendering of the microfluidic design. This draft includes a placeholder for the DEP sorter.

To model the electrohydrodynamics and fluid flow in our microfluidic device, we used the COMSOL Multiphysics software's microfluidics module. The model was built in a series of stages, beginning with the simplest case of single-phase fluid flow through a microfluidic channel. In this paper, we first detail the process involved in modeling a dielectrophoresis (DEP) sorter that separates CTCs from the rest of the peripheral blood mononuclear cells (PBMCs). CTCs are the cells that have intravasated from a primary tumor and into the bloodstream. These cells can then extravasate at a secondary site and establish a secondary tumor, known as metastasis. This DEP sorter can be used to separate the CTCs for downstream analysis, like identifying genetic hallmarks that may aid in the development of novel drug targets.

DEP is an electrokinetic phenomenon in which a uniform electric field exerts a force on a dielectric particle. The intrinsic dielectric properties of circulating tumor cells allow for their isolation from whole blood without the need for extraneous cellular markers, which enables more accurate downstream analysis.

Although we rely on an external pump to regulate the microfluidic fluid flow to mimic the heartbeat, we have simplified this COMSOL model to have linear non-Newtonian laminar fluid flow and we did not consider the potential for blood clots to form within the channels. Furthermore, we modeled the two-dimensional case because the three-dimensional case was too time intensive to rapidly iterate upon.

A prototype of a functioning fluid flow model prior to multiphysics modeling with dielectrophoresis is shown in Figure 3. Parameters were modified from targets to enhance visibility and troubleshooting as an appropriate field model was selected to properly separate CTCs from red blood cells (RBCs) as a proof-of-concept. This particular model successfully implements laminar flow and particle tracing. While we were able to make some progress on developing a DEP sorter, the models consistently returned errors and failed to converge properly once we attempted to integrate Multiphysics models involving three or more modules. Furthermore, using values from the literature to model this system sometimes returned a null set of

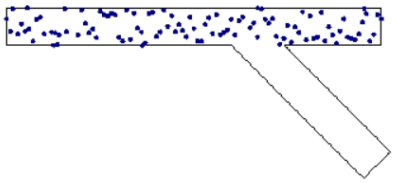

Figure 3. Particle trajectories(RBC and CTCs) under laminar fluid flow conditions as modeled in COMSOL.

particles or other unexpected behavior. Regardless, laminar fluid flow and particle behavior was as expected in this simple model.

For the purposes of learning more about the system we were trying to model, we identified an existing dielectrophoresis sorter from the COMSOL library (designed to separate red blood cells from platelets) and attempted to modify the parameters to separate CTCs instead.[13] The model uses three different physics interfaces: creeping flow to model fluid flow; electric currents to model the electric field in the sorter; and particle tracing to model the trajectories of CTCs and red blood cells (RBCs) when the dielectrophoretic forces are applied. We started with parameters specified in Low et. al., 2015, and modified them iteratively in an attempt to gain an understanding of the model.[14] This was met with moderate success.

We attempted to model a blood-brain barrier (BBB) by modeling multiphase flows through porous media. However, the model itself either had simplified parameters that failed to generate meaningful results or the models were more complex but simply wouldn't converge. We propose potential explanations for our difficulty modeling complex behavior in COMSOL, as well as potential solutions going forward, in Figure 4.

We attempted to model dielectrophoresis sort behavior using Python. To generate the synthetic data for the dielectrophoresis sorter, parameters were taken from a paper that used a dielectrophoretic method to sort cells.[15] These parameters included the shape of the electric field generator, electric field,

Possible Cause	Potential Fix
Very slow convergence	BU Shared Computing Cluster; Wait
Mean or estimated parameters makes initial conditions too far from convergence in the model	Modify with alternate experimental or literature-based parameters
Lack of fine-tuning the differential equations	Research reasonable next steps
Modeling a complex interface between biology and the microfluidic device with too many unknowns	Identify appropriate approximations to allow for convergence

Figure 4. COMSOL challenges and proposed solutions.

voltage, and flow rate of the cells. However, the paper and the experiment mostly focused on using the different cells as parameters and kept the experimental setup parameters for the dielectrophoresis sorter constant. Therefore, the paper's experimental setup parameters were used as the mean in a normal distribution, and random data was sampled from this distribution in order to substitute for the varying parameters and their results. This data was formed into a csv file and separated into training data and test data.

The data was then fed into a linear regression algorithm using gradient descent. A regression was chosen because it could be used to find the weights of every parameter and determine which parameters mattered most during the experimental setup. Regression also allows for a prediction of the results using the learned parameters. The parameters of the data are all given weights and the algorithm attempts to predict the outcome based on given parameters. The prediction's accuracy is measured, recorded, and turned into a loss function that shows how far off the prediction is from the actual outcome. The prediction's accuracy increases and the loss function decreases as the algorithm adjusts the parameter weights using gradient descent. Eventually, when the algorithm reaches a local minimum, adjustments are stopped and the resulting parameter weights are given. These weights are used to predict outcomes from test data and determine the training error. Although the data was not very meaningful as it was synthesized based on only one paper's experimental setup, the machine learning model should still prove valuable as it could easily be modified to fit new meaningful data of similar parameters.

In lieu of using COMSOL data to train machine learning algorithms, we created a mathematical model of metastasis as can be studied in our microfluidic design. To generate artificial data with physiological relevance, we created a system of equations describing the process of metastasis. For this model, we assume that the cancer is staged such that CTCs exist. In this model, the tumor will release a constant level of cells (T) into the bloodstream, which is scaled by the amount of angiogenesis (F). Parameter I represents the number of CTCs eliminated via an immune response. The entire formula is scaled by parameter P, representing the permeability of the blood-brain barrier. C represents the level of CTCs. This information is summarized in the model below and depicted in Figure 5.

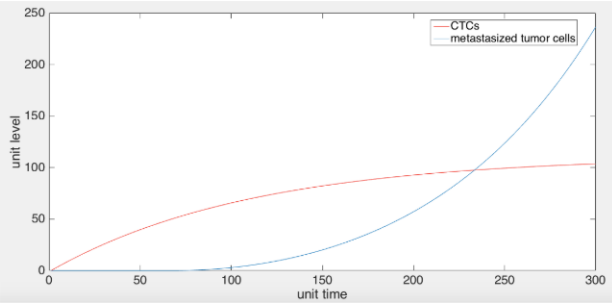

Figure 5. Metastasis Model.

T = 100: Cancer cells entering circulation per unit time
Ct = 50: Threshold of CTCs required to pass blood-brain barrier and establish a metastatic site
C: Level of circulating tumor cells
M: Level of metastasized tumor cells
I: Level of immunity (% of CTCs eliminated by T cells)
P: Permeability of the blood barrier
F: Proliferation of the capillaries through the tumor (angiogenesis)

$$\frac{dC}{dt} = P(FT - IC)$$

$$\frac{dM}{dt} = \begin{cases} 0 & if\ C < Ct \\ P(C - Ct + M) & if\ C > Ct \end{cases}$$

We model metastasis by setting a threshold for CTCs to extravasate into an organ before growing exponentially. M represents the level of metastasized tumor cells, which plateaus at the end of 300 rounds (representing the total level of potential metastasis). We also add a gaussian noise with variance of 100 to each level of metastasis to mimic nature.

In order to train a multiclass classifier, we have to categorize the spread of cancer into three classes: low, mid, and severe. We established these thresholds at 1000 and 10,000. Finally, we defined the range of the three parameters F, P and I, and ran 1000 simulations with values of parameters randomly chosen from the range. This captures what we might expect to see in microfluidic models or even real patient data. We recorded the three parameters in X data and the metastasis level in Y labels. We used 80% of the data as the training set and the rest as the testing set. Then we created a machine learning algorithm that could read in the X data (consisting of three parameters) and output the predicted label (which should be equal to the testing label).

We first tried the k-nearest neighbors classifier, which labels testing data based on proximity metrics from the training data. However, the testing error was high (~57%). Because the three parameters would either be positively or negatively correlated with the level of metastasis, we implemented bidirectional decision stumps with boosting instead. Decision stumps are weak binary learners that select one parameter and a threshold and categorize all data points above it as negative and all below it as positive. In order to make it bidirectional, we expanded the parameters to six by flipping the three original ones into the other three so both positive and negative correlations are accounted for. Then we trained three boosting algorithms to strengthen the decision stumps to recognize each class over the rest of data. For example, the first boosting algorithm will give positive label to all data it categorized as class low and negative label for every other classes, while the second algorithm recognized class mid, and the third one for class severe. For

Figure 6. Training and testing error from machine learning algorithm.

each testing data, we will compare the result of three algorithm and choose the label of the classifiers with the most positive margin. For a binary classifier, margin represents the level of confidence in its classification. Even if two algorithms give the same positive label, the one with higher margin will determine the class of that data.

This approach was successful. With only 100 boosting rounds, the testing error was below 5% (Figure 6). This model only consists of three parameters, but it could be scaled up to hundreds as scientist design more sophisticated and realistic microfluidic models that more closely mimic human physiology. Then we could train the classifier with thousands of microfluidic data points and use it to investigate novel drug effects and provide diagnostic and prognostic data in real patients.

This proposed microfluidic device (and associated characterizations) will aid research in the physiology and etiology of cancer metastasis and provide a modifiable biologically-inspired platform in which to test anti-metastatic drug candidates.

Conflicts of interest

There are no conflicts to declare.

References

1 P. S. Steeg, *Nat. Rev. Cancer*, 2016, 16, 201–218.
2 R. R. Langley and I. J. Fidler, *Endocr. Rev.*, 2007, 28, 297–321.
3 Z. Werb and P. Lu, *Cancer J. (United States)*, 2015, 21, 250–253.
4 X. Zhang, Z. Chen and Y. Huang, *Biomicrofluidics*, , DOI:10.1063/1.4907982.
5 European Collection of Authenticated Cell Cultures, *Cell line profile MDA-MB-231 (ECACC catalogue no. 92020424)*.
6 T. E. Park, N. Mustafaoglu, A. Herland, R. Hasselkus, R. Mannix, E. A. FitzGerald, R. Prantil-Baun, A. Watters, O. Henry, M. Benz, H. Sanchez, H. J. McCrea, L. C. Goumnerova, H. W. Song, S. P. Palecek, E. Shusta and D. E. Ingber, *Nat. Commun.*, 2019, **10**, 1–12.
7 J. Kong, Y. Luo, D. Jin, F. An, W. Zhang, L. Liu, J. Li, S. Fang, X. Li, X. Yang, B. Lin and T. Liu, *Oncotarget*, 2016, **7**, 78421–78432.
8 A. Lucci, C. S. Hall, A. K. Lodhi, A. Bhattacharyya, A. E. Anderson, L. Xiao, I. Bedrosian, H. M. Kuerer and S. Krishnamurthy, *Lancet Oncol.*, 2012, **13**, 688–695.
9 K. Stoletov, H. Kato, E. Zardouzian, J. Kelber, J. Yang, S. Shattil and R. Klemke, *J. Cell Sci.*, 2010, **123**, 2332–2341.
10 S. Bersini, J. S. Jeon, G. Dubini, C. Arrigoni, S. Chung, J. L. Charest, M. Moretti and R. D. Kamm, *Biomaterials*, 2014, **35**, 2454–2461.
11 S. A. Brooks, U. Schumacher, N. S. Brown and R. Bicknell, in *Metastasis Research Protocols*, Humana Press, 2003, pp. 047–054.
12 R. Sanka, J. Lippai, D. Samarasekera, S. Nemsick and D. Densmore, *Sci. Rep.*, 2019, **9**, 1–10.
13 COMSOL, Dielectrophoretic Separation of Platelets from Red Blood Cells, https://www.comsol.com/model/dielectrophoretic-separation-of-platelets-from-red-blood-cells-17013, (accessed 30 April 2020).
14 Wan Shi Low and Wan Abu Bakar Wan Abas, *Biomed Res. Int.*, , DOI:10.1155/2015.
15 M. Punjiya, H. R. Nejad, J. Mathews, M. Levin and S. Sonkusale, *Sci. Rep.*, 2019, **9**, 1–11.